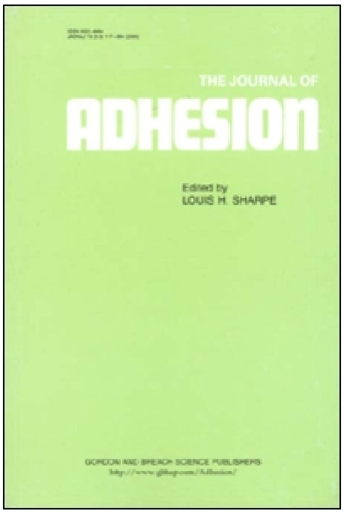

The Journal of Adhesion
Publication details, including instructions for authors and subscription information:
http://www.informaworld.com/smpp/title~content=t713453635

Theory and Analysis of Fracture Energy in Fiber Reinforced Composites

D. H. Kaelble[a]
[a] North American Rockwell Science Center, Thousand Oaks, California, U.S.A.

To cite this Article Kaelble, D. H.(1973) 'Theory and Analysis of Fracture Energy in Fiber Reinforced Composites', The Journal of Adhesion, 5: 3, 245 — 264
To link to this Article: DOI: 10.1080/00218467308075022
URL: http://dx.doi.org/10.1080/00218467308075022

J. Adhesion, 1973, Vol. 5, pp. 245–264

Printed in Northern Ireland

Theory and Analysis of Fracture Energy in Fiber Reinforced Composites†

D. H. KAELBLE

North American Rockwell Science Center, Thousand Oaks, California 91360, *U.S.A.*

(*Received January* 8, 1973)

A micro-mechanics model is developed to analyze the stress distributions and fracture energies associated with crack propagation and fiber pull-out in reinforced composites. The stress and work mechanisms of interfacial debonding, fiber deformation, and the frictional work of fiber pull-out are considered as semi-independent contributions to fracture toughness. The theoretical expressions of Cottrell for frictional work W_F and Outwater and Murphy for fiber deformational work W_D are obtained as special relations in a general relation for the total work $W_T = W_S + W_F + W_D$ where W_S defines the matrix shear work for interfacial debonding of fiber and matrix. Three dimensional diagrams of fracture energies W_T, W_S, or W_F versus interfacial shear bond strength λ_0 and frictional shear stress λ_F identify regions of optimized fracture energy. The influence of environmental degradation of bond strength upon fracture energy is analyzed in terms of the theory.

INTRODUCTION

The fracture energy in fiber reinforced composites, where the crack propagates perpendicular to the axis of fiber reinforcement, is accounted for by micro-mechanics models for fiber pull-out.[1–5] The major emphasis in the theories of Cottrell, Cooper, and Kelly involves frictional work W_F expended in extracting the fiber from the matrix.[1–4] Outwater and Murphy consider the deformational work W_D contributed by the tensile strain of the fiber in the region of interfacial debonding.[5] Linear elastic analysis for the shear stress distributions around bonded fibers in a pull-out geometry is provided

† Presented at the Symposium on "Interfacial Bonding and Fracture in Polymeric, Metallic and Ceramic Composites" at The Univ. of California at Los Angeles, Nov. 13–15, 1972. This Symposium was jointly sponsored by the Polymer Group of So. California Section, ACS and Materials Science Department, U.C.L.A.

by Greszczuk[6] and Lawrence.[7] An elastic-plastic analysis for the case of an elastic fiber bonded to a ductile matrix has been developed by Lin, Salinas and Ito.[8] Recent experimental studies of interface contributions to fracture energy strongly suggest the need to consider both the shear bond strength λ_0 and the frictional shear stress λ_F between fiber and matrix in a more detailed analysis of fracture energy.[9,10]

This discussion develops a generalized model for fracture energy in uniaxially reinforced composites. One objective of the analysis is to provide an analytic definition of the role played by variable magnitudes of the interfacial shear stresses λ_0 and λ_F, in conjunction with other composite properties, upon fracture energy. A second objective is to isolate the separate contributions of matrix shear work W_S, interfacial frictional work W_F, and fiber tensile work W_D on the total fracture energy $W = W_S + W_F + W_D$. Significant variables to be analyzed are identified in Table I.

TABLE I
Nomenclature of significant variables

Forces	
p	= fiber pull out force
q	= incremental shear force at bonded interface
f	= incremental frictional force at debonded interface
Stresses	
λ_S	= shear stress at bonded interface
λ_0	= boundary shear stress at fracture
λ_F	= frictional shear stress
σ_b	= fiber tensile strength
Moduli	
E	= fiber Young's modulus
G	= matrix shear modulus
Works	
W_S	= work for shear debonding
W_F	= frictional work for fiber pull-out
W_B	= tensile work of fiber deformation
W	= total work of fiber pull-out
General	
V	= volume fraction of fiber
A	= cross section area of unit cell
L_F	= fiber pull-out length
L_b	= fiber debond length
P_b/A	= fracture force/unit area
W/A	= fracture work/unit area
α	= shear stress concentration factor
r_0	= fiber radius
a	= r_1-r_0 = thickness of the matrix annulus

FRACTURE STRESS AND ENERGY

The square and hexagonal cells for uniaxial packing of uniform circular fibers are shown in Table II along with significant parameters related to

TABLE II
Packing geometries in regular uniaxial fiber arrays

Lattice type	Square	Hexagonal
Unit geometry	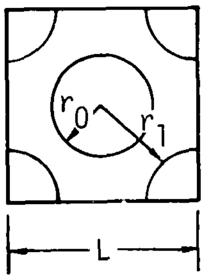	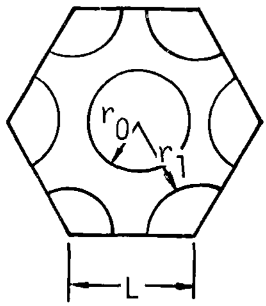
Fibers/Unit Cell	2.0	3.0
Fiber volume fraction (v)	$2\pi(r_0/L)^2$	$1.1548\pi(r_0/L)^2$
Unit Cell Area (A)	$2\pi r_0^2/V$	$3\pi r_0^2/V$
$a = (r_1 - r_0)$	$r_0[(\pi/V)^{1/2} - 2]$	$r_0[1.074(\pi/V)^{1/2} - 2]$
v at $(r_1 - r_0) = 0$	0.785	0.906

fiber packing. The unit cell models of Table II illustrate a circular fiber centered within the partial cross sections of nearest neighbor fibers. The fiber separation distance $a = r_1 - r_0$ describes an annular region of matrix about the central fiber. A convenient basis for calculation of the shear stresses when the central fiber is subject to a pull out force P is illustrated in the schematics of Figure 1.

The upper view of Figure 1 shows a cross section of the central fiber of diameter $2r_0$ imbedded in an annular layer of matrix of thickness $a = (r_1 - r_0)$. A length L of the fiber is debonded but interacts with the matrix to provide a total frictional force $\sum f$. The interface to the left of the bond boundary at $x = 0$ interacts via bonding shear forces whose summation is $\sum q$. Since the applied force and the reactive interfacial forces are centrally symmetric, the moments of force vanish and the equation for steady state equilibrium is:

$$P = \sum f + \sum q \tag{1}$$

The lower schematic of Figure 1 describes the balance of forces for an incremental length dx of fiber at some distance $(-x)$ to the left of the bond boundary at $x = 0$. By assuming the fiber is continuous in the bonded region

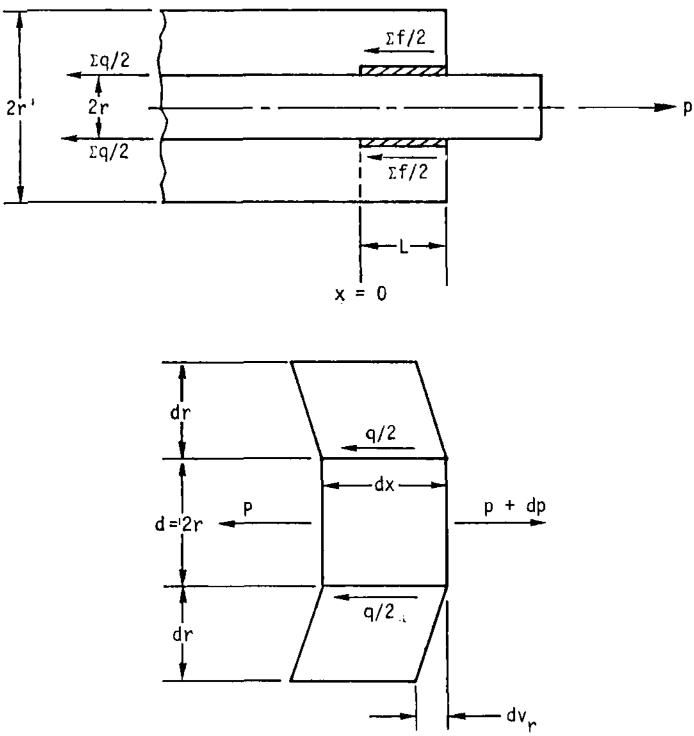

FIGURE 1 Schematic of forces and displacements about the central fiber in a unit cell of composite material.

so that $q = 0$ at $x = -\infty$ the derivation of Appendix A provides the following relation for the bonded shear stress at the fiber-matrix interface when $\sum f = 0$:

$$\lambda_s = \frac{\alpha P \exp(\alpha x)}{2\pi r_0} \tag{2}$$

or:

$$\lambda_s = \lambda_0 \exp(\alpha x) \tag{3}$$

where

$$\alpha = (2G/E)^{1/2}/r_0 \ln(r_1/r_0) \tag{4}$$

The bond shear stress function is expressed in Eq. (2) and Eq. (3) as a simple exponential decay form with maximum shear stress λ_0 at the bond boundary ($x = 0$). The stress decay factor α has dimensions of reciprocal length and represents a measure of shear stress concentration.

Substituting the relation $\lambda_s = -q/2\pi\,\mathrm{d}x$ into Eq. (2) and rearranging into integral form provides the following relation:

$$\sum q = -2\pi r_0 \lambda_0 \int_{x=0}^{-\infty} \exp(\alpha x)\, \mathrm{d}x = P_S$$

Evaluating this integral provides the relation

$$P_S = 2\pi r_0 \lambda_0/\alpha \qquad (5)$$

where P_S is the pull-out force required to generate a critical boundary stress λ_0 for interfacial debonding. The work of propagating failure a distance L into the matrix is:

$$W_S = P_S L = 2\pi r_0 \lambda_0 L/\alpha \qquad (6)$$

Eqs. (5) and (6) provide preliminary expressions for the force and energy requirements for interfacial debonding due to shear of the matrix.

When a constant frictional stress $\lambda_F = f/2\pi r_0\, \mathrm{d}x$ exists between fiber and matrix in the region L of debonding the force summation $\sum f$ is described by the following relation:

$$\sum f = 2\pi r_0 \lambda_F L = P_F \qquad (7)$$

When a debonded fiber breaks a distance L_F inside the matrix the frictional work of pull-out is given as:

$$W_F = -\int_{L_F}^{L=0} P_F\, \mathrm{d}L = \pi r_0 \lambda_F L_F^2 \qquad (8)$$

Although more complicated frictional stress and work functions may be postulated, Eqs. (7) and (8) are adequate for this analysis.

An additional contribution to the work of interfacial fracture involves the elastic work of tensile deformation W_D in the fiber length L which is lost at the instant of fracture. Outwater and Murphy consider the case for constant frictional stress $\lambda_F = f/2\pi r_0\, \mathrm{d}x$ to show that:[5]

$$W_D = \frac{\pi r_0^2}{2E} \int_{L=0}^{L} \left(\sigma - \frac{2\lambda_F L}{r}\right)^2 \mathrm{d}L \qquad (9)$$

where σ is the tensile stress in the unconstrained fiber. Evaluating the above integral and substituting the relation $L = r_0\sigma/2\lambda_F$ provides the following relation:

$$W_D = \frac{\pi r_0^2 \sigma^2 L}{6E} \qquad (10)$$

for the fiber deformational work.

The above relations identify two contributions to the total pulling force P as:

$$P = P_S + P_F \qquad (11)$$

and three contributions to the work of pull out as:

$$W = W_S + W_F + W_D \tag{12}$$

Combining Eqs. (5) and (6) provides the following statement:

$$P = 2\pi r_0[(\lambda_0/\alpha) + \lambda_F L] \leqslant \pi r_0^2\sigma_b \tag{13}$$

The inequality in Eq. (13) describes the upper limit for the pull-out force P in terms of the tensile strength σ_b of the fiber. Rearrangement of Eq. (13) provides a new relation for the maximum debond length L_b, when $P = \pi r_0^2\sigma_b$, as follows:

$$L_b = (1/\lambda_F)[(r_0\sigma_b/2) - (\lambda_0/\alpha)] \geqslant 0 \tag{14}$$

By applying a similar criteria for the works of fracture, that $P = P_b = \pi r_0^2\sigma_b$, $L = L_b$, and $\sigma = \sigma_b$ the following special relations result:

$$W_{Sb} = 2\pi r_0\lambda_0 L_b/\alpha \tag{15}$$

$$W_{Bb} = \pi r_0^2\sigma\,^2 L_b/6E \tag{16}$$

$$W_{Fb} = \pi r_0\lambda_F L_F^2 \tag{17}$$

$$W_b = W_{Sb} + W_{Bb} + W_{Fb} \tag{18}$$

as the maximum works for fracture per unit cell.

In order to evaluate the specific performance per unit area A of composite cross section area, it is convenient to incorporate functions of fiber volume fraction V into the above relations. Utilizing the relations of Table II it is readily shown that Eq. (14) can be reexpressed as:

$$L_b = \frac{r_0}{\lambda_F}\left[\frac{\sigma_b}{2} - \lambda_0(E/2G)^{1/2}f_1(V)\right] \geqslant 0 \tag{19}$$

The specific fracture work W/A involving the three contributions defined by Eq. (15) through Eq. (18) for the respective W_{Sb}, W_{Bb}, and W_{Fb} contributions becomes:

$$\frac{W_b}{A} = \lambda_0\left(\frac{E}{2G}\right)^{1/2} L_b f_1(V) f_2(V) + \frac{\sigma_b^2}{12E} L_b f_2(V) + \frac{\lambda_F L_F^2 f_2(V)}{2r_0} \tag{20}$$

$$= (W_{Sb} + W_{Bb} + W_{Fb})/A$$

The fracture stress $P_b = \pi r_0^2\sigma_b$ per unit area A is given by the following relation:

$$\frac{P_b}{A} = r_0\sigma_b f_3(V) \tag{21}$$

For the square fiber packing with $0 \leqslant V \leqslant 0.785$ the volume fraction functions are:

$$f_1(V) = \ln(r_1/r_0) = \{\ln[(\pi/V)^{1/2} - 1]\}^{1/2} \tag{22}$$

$$f_2(V) = V \tag{23}$$

$$f_3(V) = (V/\pi)^{1/2} \tag{24}$$

Hexagonal packing with $0 \leqslant V \leqslant 0.906$ describes volume functions:

$$f_1(V) = \ln(r_1/r_0) = \{\ln[1.074(\pi/V)^{1/2} - 1]\}^{1/2} \tag{25}$$

$$f_2(V) = 2V/3 \tag{26}$$

$$f_3(V) = 2(V/\pi)^{1/2}/3 \tag{27}$$

Other types of irregular or random packing would be expected to provide volume fraction functions intermediate between those developed above for square and hexagonal packing.

OPTIMIZATION OF FRACTURE ENERGY

A clarification of the factors which produce optimization of the fracture energy in reinforced composite materials remains as one of the important current objectives in composite design. The influence of the interfacial shear stresses λ_0 and λ_F defined in the present model may be graphically illustrated by assuming constant values for the parameters tabulated in Table III

TABLE III

Typical physical properties of a uniaxially reinforced graphite fiber-polymer matrix composite material

fiber radius $= r_0 = 2.10^{-4}$ in $\simeq 5\ \mu$m
fiber tensile strength $= \sigma = 2.10^5$ psi
fiber Young's modulus $= E = 5.10^7$ psi
fiber volume fraction $= V = 0.50$
matrix shear modulus $= G = 1.5 \,.\, 10^5$ psi
fiber packing = square (4 nearest neighbors)
volume fraction functions: $f_1(V) = 0.64, f_2(V) = 0.50, f_3(V) = 0.266$

and solving for L_b defined by Eq. (19) and the specific fracture energies defined in Eq. 20. The physical properties identified in Table III are representative of a uniaxially reinforced graphite fiber-epoxy matrix composite material.

Calculations involving Eq. (19) provide the response surface of interface debonding L_b, plotted on the abscissa of Figure 2, where shear debonding stress $0 \leqslant \lambda_0 \leqslant 12000$ psi and the frictional stress $500 \leqslant \lambda_F \leqslant 6000$ psi

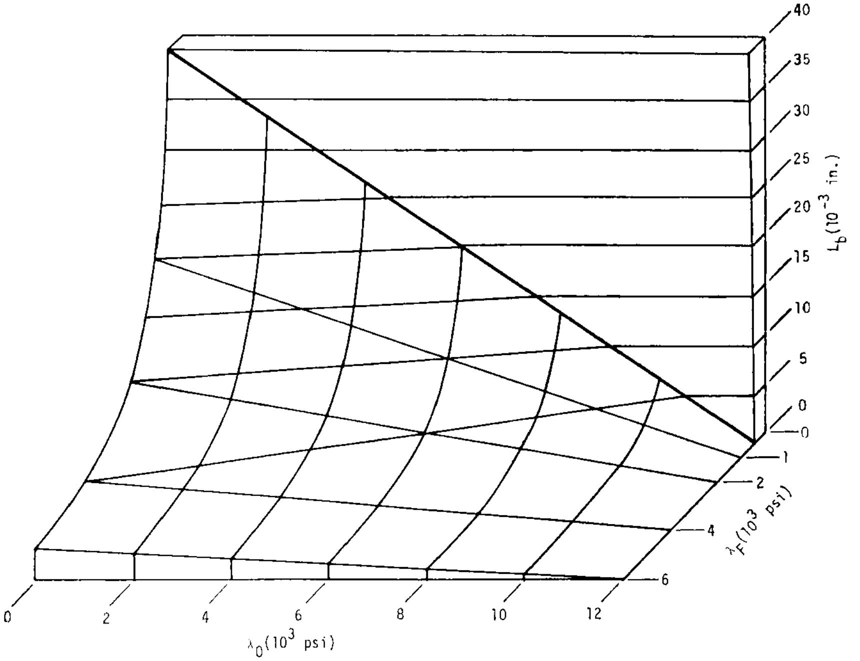

FIGURE 2 Response surface of fiber debond length L_b (ordinate) for variable fiber-matrix shear strength λ_0 and interface frictional stress λ_F.

One clear fashion in which the present model predicts minimized fractured energy $W_b/A = 0$ is defined by Eq. (19) for the following inequality:

$$2\lambda_0(E/2G)^{1/2}f_1(V) \geqslant \sigma_b \qquad [L_b = 0] \tag{28}$$

which points out that the composite described by Table III will display $L_b = 0$ when $\lambda_0 \geqslant 12100$ psi. Equation (28) thus provides an initial design criteria which places an upper limit on λ_0 where optimized fracture energy is a design criteria. It is important that the result obtained in Eq. (28) does not depend upon the value of the frictional stress λ_F. The left boundary of Figure 2, where $\lambda_0 = 0$, graphs the prediction for L_b defined by the Cottrell theory:[1]

$$L_b = \frac{\sigma_b r_0}{2\lambda_F} = \frac{L_c}{2} \qquad [\lambda_0 = 0] \tag{29}$$

where L_c is termed the critical fiber length. The generalization for predicted values of L_b provided by the present model is represented in Figure 2 by the response surface which interconnects the special cases defined by Eq. (28) and (29).

The response surface for the frictional work per unit area W_{Fb}/A for the maximum value of frictional pull out length $L_F = L_b$ is presented in Figure 3 for the stress ranges shown previously for L_b (see Figure 2). The pertinent terms of Eq. (20) provide the following relation:

$$\frac{W_{Fb}}{A} = \frac{f_2(V)\lambda_F L_F^2}{2r_0} \tag{30}$$

By assuming $L_F = L_b$ and substituting Eq. (19) into Eq. (30) we obtain the following special relation:

$$\frac{W_{Fb}}{A} = \frac{f_2(V)r_0}{2\lambda_F}\left[\frac{\sigma_b}{2} - \lambda_0\left(\frac{E}{2G}\right)^{1/2} f_1(V)\right]^2 \qquad [L_f = L_b] \tag{30a}$$

which defines the response surface of Figure 3. The response surface for Figure 3 predicts that the frictional pull-out work maximizes when both λ_0

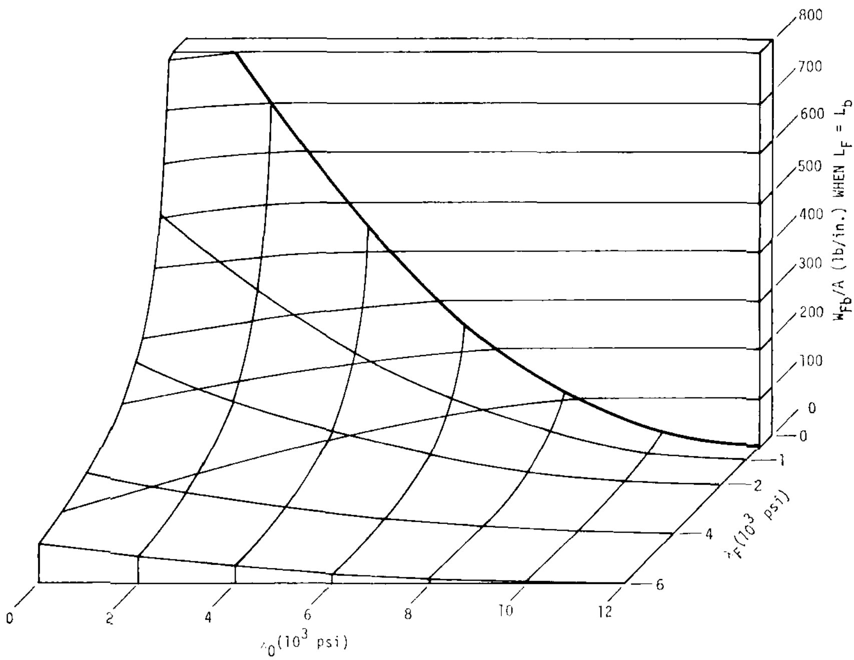

FIGURE 3 Response surface for maximized frictional shear work per unit area W_{Fb}/A (ordinate) for variable shear stresses λ_0 and λ_F when $\lambda_F = L_b$.

and λ_F are reduced toward minimum values. The Cottrell theory for fracture energy can be stated in the following form:[1]

$$\frac{W_b}{A} = \frac{Vr_0\sigma_b^2}{12\lambda_F} \qquad [\lambda_0 = 0] \tag{31}$$

The left boundary curve of Figure 3 where $\lambda_0 = 0$ is similar to the Cottrell criteria, Eq. (31), for total fracture energy. The refinement in the present argument again relates to the capability to calculate the independent influence of the interfacial shear strength λ_0 in minimizing the value of W_{Fb}/A toward zero for the condition $L_b = 0$ defined by Eq. (28).

The shear work of matrix debonding W_{Sb}/A is given by Eq. (20) as:

$$\frac{W_{Sb}}{A} = \lambda_0 \left(\frac{E}{2G}\right)^{1/2} L_b f_1(V) f_2(V) \tag{32}$$

By substituting Eq. (19) into Eq. (32) we obtain the following detailed statement:

$$\frac{W_{Sb}}{A} = f_1(V) f_2(V) r_0 \left(\frac{E}{2G}\right)^{1/2} \frac{\lambda_0}{\lambda_F}\left[\frac{\sigma_b}{2} - \lambda_0\left(\frac{E}{2G}\right)^{1/2} f_1(V)\right] \tag{32a}$$

The response surface for W_{Sb}/A shown in Figure 4 maps the influence of both

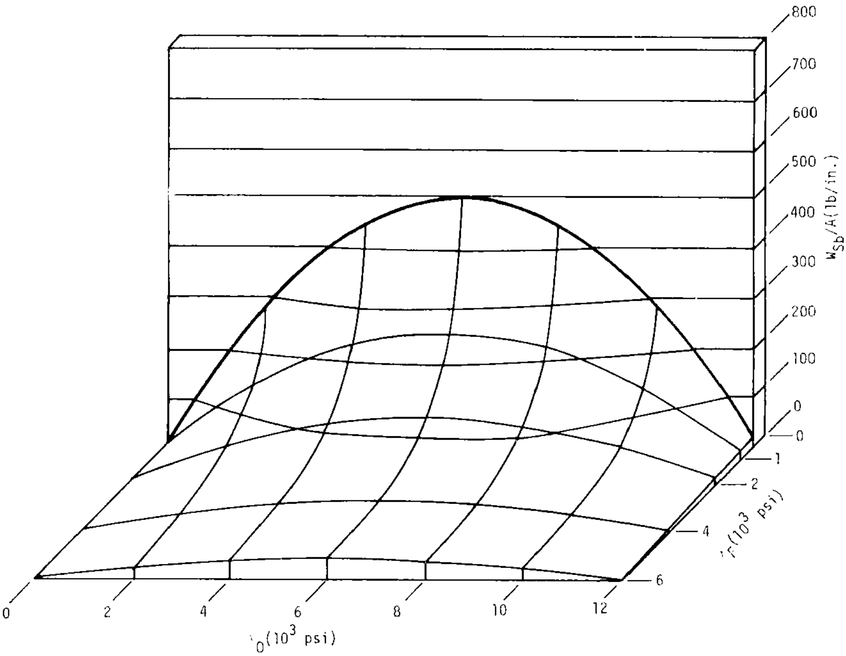

FIGURE 4 Response surface for matrix shear work per unit area W_{Sb}/A (ordinate) for variable stresses λ_0 and λ_F.

λ_F and λ_0 for the model composite described by Table III. Inspection of Figure 4 shows that W_{Sb}/A optimizes at intermediate values of $\lambda_0 \simeq 6000$ psi and $\lambda_F \leqslant 2000$ psi. The response surface generated by Figure 4 identifies a new mechanism for optimizing fracture energy not described in previous theory.

The fracture energy due to bulk deformation of the fiber at fracture is defined from Eq. (20) as follows:

$$\frac{W_{Bb}}{A} = \frac{f_2(V)\sigma_b^2}{12E} L_b \tag{33}$$

For the model composite described by Table III it is easily shown that W_{Bb}/A is negligible compared to the sum $(W_{Fb} + W_{Sb})/A$. For the stress ranges shown in Figure 2 the maximum value $W_{Bb}/A = 1.34$ lb/in occurs at $\lambda_0 = 0$ and $\lambda_F = 500$ psi.

The response surface of Figure 5 expresses the maximum value for the

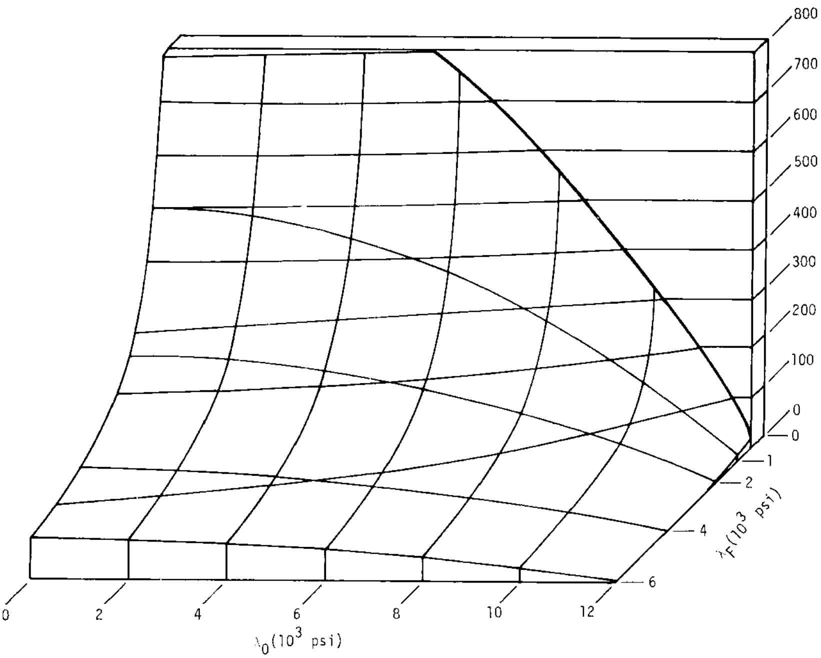

FIGURE 5 Response surface for combined works per unit area $(W_{Sb} + W_{Fb})/A$ for variable shear stresses λ_0 and λ_F.

calculated fracture energy for the model composite, where $W_b/A \simeq (W_{Fb} + W_{Sb})/A$, for the special case where $L_F = L_b$. By summing the region of optimized fracture energy previously shown for the frictional (see Figure 3) and shear debonding (see Figure 4) a new broadened region of high fracture energy where $0 \leqslant \lambda_0 \leqslant 6000$ and $\lambda_0 \leqslant 2000$ is presented in Figure 5. In a real composite system where the statistics of fiber fracture provides a distribution for L_F where $0 \leqslant L_F \leqslant L_b$ the fracture energies will lie between the predictions of Figures 4 and 5.

The curves of Figure 6 illustrate the above point for the model composite of Table III where $\lambda_F = 2000$ psi. The upper curves of Figure 6 show the single and combined contributions for W_{Sb}/A and W_{Fb}/A for the maximum condition $L_F = L_b$. The middle curves show the intermediate case where the fibers break an average distance $L_F = L_b/2$. The lower curves present the extreme $L_F = 0$. When L_F is reduced so that $L_F < L_b$ the stress criteria for optimum fracture energy is immediately dominated by the W_{Sb}/A contribution. Considering that the fibers may tend to break so as to produce $L_F \simeq L_b/2$ places a new emphasis on optimizing the combination of factors in Eq. (32a) which maximize W_{Sb}/A.

Inspection of Eq. (32a) shows that W_{Sb}/A is optimized when the product $f_1(V) \cdot f_2(V)$ is maximized. The lower curve of Figure 7 plots the separate functions of $f_1(V)$ and $f_2(V)$ for the square fiber packing described by Table III. The upper curve of Figure 7 shows a broad maximum $f_1(V)f_2(V) \geqslant 0.30$ at intermediate fiber volume fraction $0.4 \leqslant V \leqslant 0.60$. The model composite described by Table III and Figure 2 through Figure 6 represent optimized W_{Sb}/A response with respect to the volume fraction $V = 0.50$ and $f_1(V)f_2(V) = 0.320$.

CORRELATION WITH EXPERIMENTAL RESULTS

One of the interesting results provided by the present model is the prediction that strong interfacial bonding, where λ_0 is beyond an optimum range, will lead to reduced values of both W_{Fb}/A and W_{Sb}/A. This finding correlates with experimental evidence that shows that good stress transmission through the composite tends to lower both impact strength and resistance to fatigue damage.[9-12]

Experimental evidence for the existance of a shear bond strength $\lambda_0 \rightarrow \lambda_F$ is available from the disc shear test discussed by Broutmann[11] and illustrated in Figure 8. In this test the primary force maximum correlates with the shear bond strength λ_0 of the present model. The subsequent resistance to pulling the fiber through the disc shaped annulus of matrix correlates with the frictional shear stress λ_F. While this test method has been applied to evaluate values of λ_0 and λ_F for glass rods of radius $r_0 = 0.5$ to 2.0 mm, it is unsuitable for composite materials such as represented in Table III. For example, single graphite fibers with $\sigma_b = 2.10^5$ psi, $r_0 = 5.0\ \mu m = 2.10^{-4}$ in and

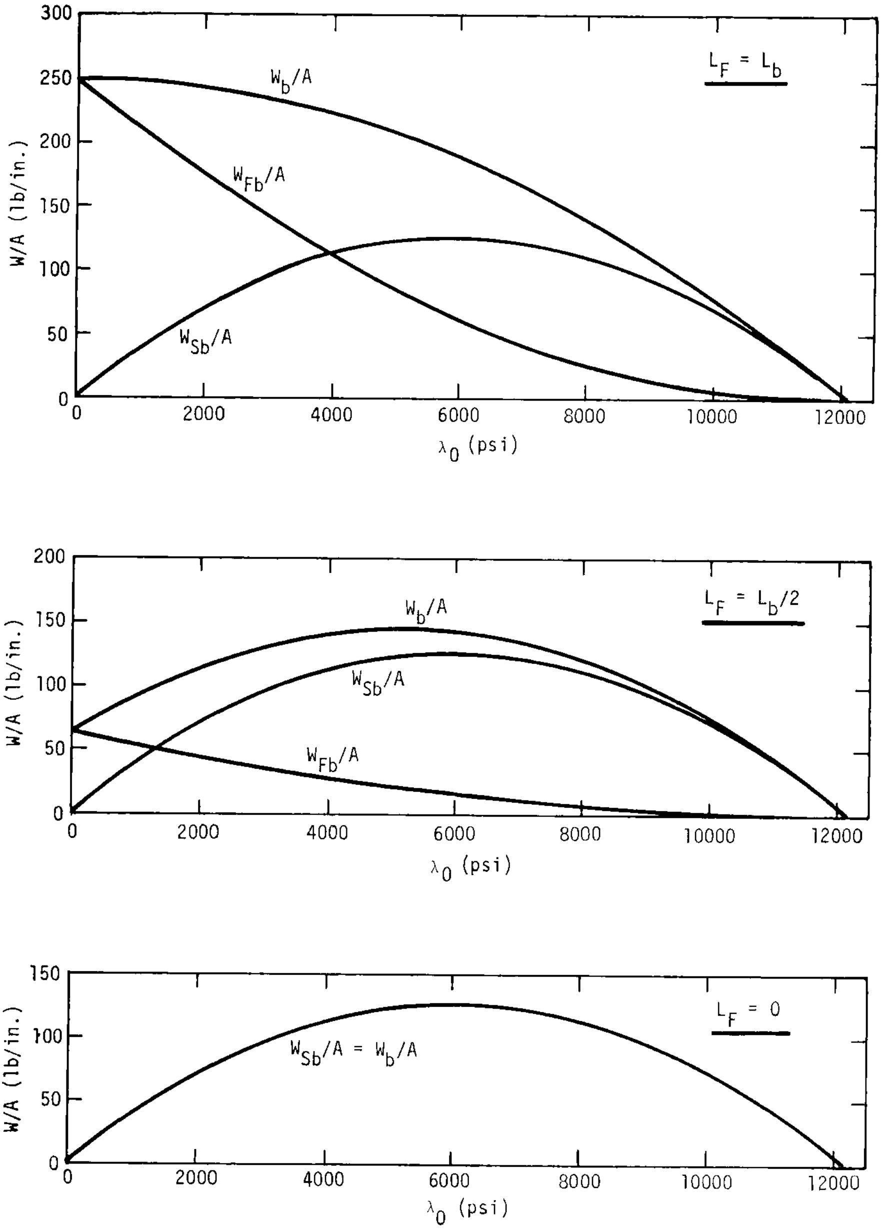

FIGURE 6 Influence of diminished fiber pull-out length $L_F \leq L_b$ upon the relative contributions of W_{Fb} and W_{Sb} to the specific fracture energy $W_b/A = (W_{Sb} + W_{Fb})/A$ for variable λ_0 and a fixed level of $\lambda_F = 2000$ psi.

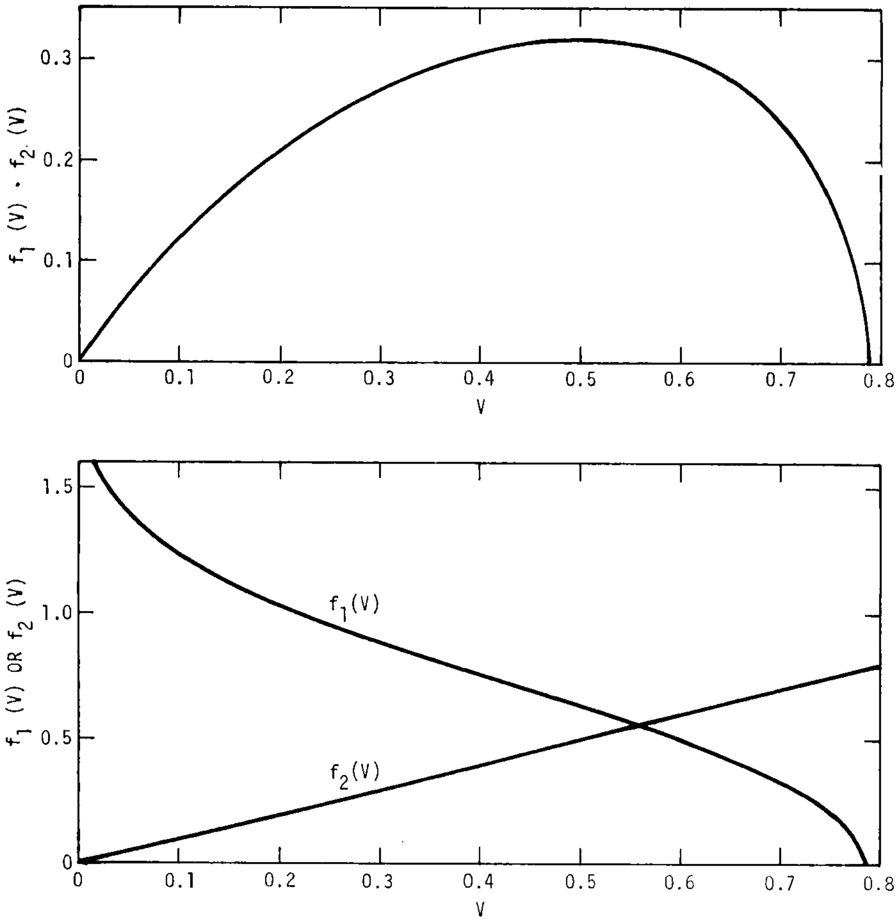

FIGURE 7 Optimization of the volume fraction functions $f_1(V)$, $f_2(V)$ and product $f_1(V) \cdot f_2(V)$ versus fiber volume fraction V.

$\lambda_0 \geqslant 1000$ psi would require a disc thickness $t < 0.002$ in which it is too small for practical testing. Through Eq. (3), the present theory points out that to maintain a smaller than 10 percent variation in shear stress λ_S a new thickness criteria $t < 0.1\ \alpha^{-1}$ is required as a further constraint on the disc geometry.

The results of a study by Harris, Beaumont, and de Ferran[9] appear to clearly correlate with the theoretical model developed in this discussion. In this study a uniaxially reinforced composite of graphite fiber, with volume fraction $V \simeq 0.40$ in a thermosetting polyester matrix was evaluated for interface contributions to fracture energy and interlaminar shear strength.

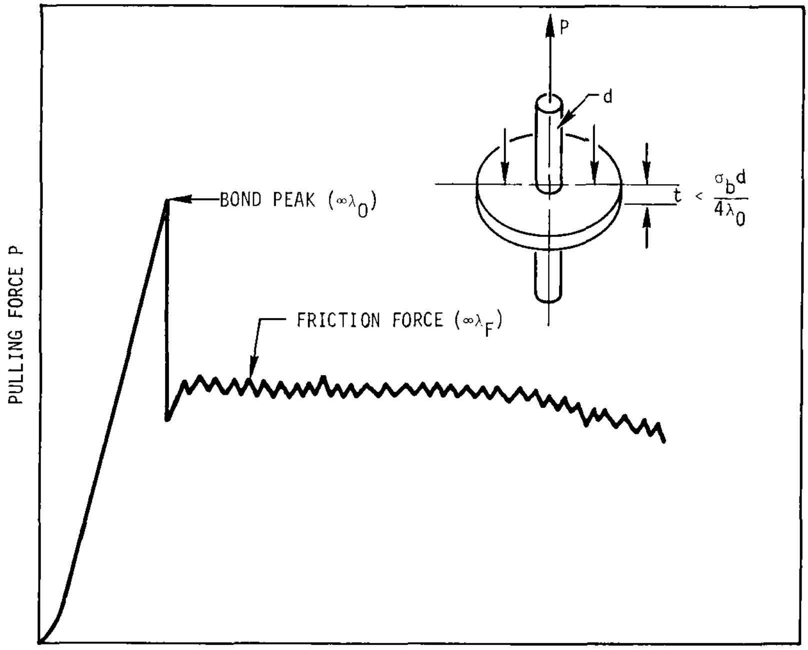

FIGURE 8 Schematic of disc shear test illustrating bond peak force ($\propto\lambda_0$) and frictiona force ($\propto\lambda_F$) — (from ref. 11).

TABLE IV
Correlation between interlaminar shear strength and fracture energy in graphite-polyester composites (data from ref. 9)

Interface treatment	Interlaminar shear strength (psi)	Fracture work	
		Charpy (lb/in)	Slow bend (lb/in)
1) untreated fiber— 7 day steam exposure	1450	—	94
2) silicone oil treated	1740	199	—
3) untreated fiber— no accelerated aging	2970	188	194
4) acid etched and brominated	3620	137–160	171–194
5) silane treated	4000	166	120
6) treated Morganite	8000	50	—

Table IV arranges the data in the order of increasing interlaminar shear strength which appears to correlate with λ_0 of the present discussion. Interface treatments (1) and (2) of Table IV were designed to weaken the fiber-matrix interface while treatments (4), (5) and (6) were designed to produce strong interfacial bonding. The plot of the fracture energy versus interlaminar shear strength shown in Figure 9 appear to correlate with the theoretical

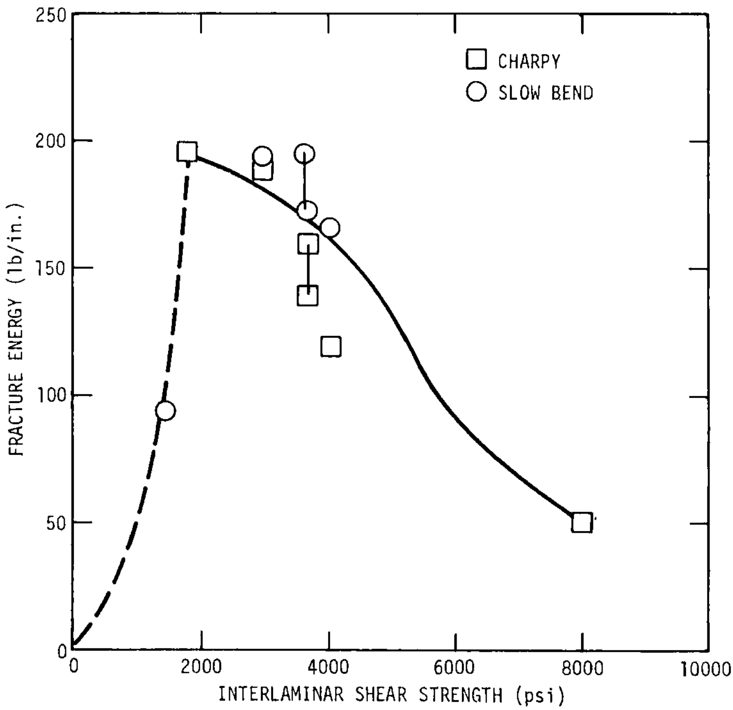

FIGURE 9 Experimental correlation between fracture energy and interlaminar shear strength for graphite fiber/polyester matrix composites—(from ref. 9).

curves of W_b/A shown in Figure 6 when $L_F \leqslant L/2$. The magnitudes of the calculated fracture energy shown by the lower curves of Figure 6 are in reasonable agreement with the experimental data of Figure 9. The theory embodied in Figure 6 also reflects the maximizing of fracture energy at intermediate bond strengths as in the data of Figure 9.

SUMMARY AND CONCLUSIONS

The effective fracture energy is decomposed in this discussion into a matrix shear work of debonding W_{Sb}, a frictional work of fiber pull-out W_{Fb}, and a work of fiber extension to break W_{Bb}. A separation of the shear debonding stress λ_0 and debonding length L_b from the frictional stress λ_F and pull-out length L_F provides greater detail to the analysis of fracture energy contributions and the design factors which lead to specific optimizations of W_{Sb} and W_{Fb}. The analysis shows that W_{Bb} is essentially negligible when compared with the sum $W_b \simeq W_{Sb} + W_{Fb}$.

Calculations based on the theoretical model identify the magnitudes of shear bond strength λ_0 and frictional stress λ_F where the W_{Sb} contribution to fracture energy are maximized and provide the dominant contribution to the total fracture energy. Adjusting the balance of fiber-matrix shear stresses λ_0 and λ_F in conjunction with fiber volume fraction V so as to maximize the W_{Sb} contribution would appear to provide a new basis for designing both stress transmitting and energy absorption properties into fiber reinforced composite materials. A particularly interesting feature in adjusting W_{Sb} to a maximized response is the feature that variations in shear bond strength λ_0 due to environmental or mechanical fatigue damage should produce only minor changes in W_{Sb}.

Acknowledgment

The writer gratefully acknowledges helpful discussions with Dr. H. L. Ho. This work was supported in part by the North American Rockwell IR and D Interdivisional Technology Program under the sponsorship of the Composites Technical Panel.

APPENDIX A: The Shear Stress Function

The condition for equilibrium of internal forces (see Figure 1) provides that:

$$dp + q = 0 \tag{A-1}$$

The fiber tensile stress σ at $L = 0$ is:

$$\sigma = P/\pi r_0^2 \tag{A-2}$$

which upon differentiation and rearrangement becomes:

$$dp = \pi r_0^2 \, d\sigma \tag{A-3}$$

The shear stress λ_r varies with radius r, where $r_0 \leqslant r \leqslant r_1$

$$\lambda_r = -q/2\pi r \, dx$$

the shear strain γ at position x and radius r is expressed in terms of shear displacement u as follows:

$$\gamma_{xr} = \mathrm{d}u_r/\mathrm{d}r$$

The matrix shear modulus G is defined as:

$$G = \lambda_r/\gamma_r = -(q/2\pi\,\mathrm{d}x)(\mathrm{d}r/r)(1/\mathrm{d}u_r)$$

The total shear displacement u_x of matrix element of length $\mathrm{d}x$ from radius r_0 to r_1 is:

$$u_x = \frac{(-q/G)}{2\pi\,\mathrm{d}x}\int_{r=r_0}^{r_1} \mathrm{d}r/r = \frac{(-q/G)\ln(r_1/r_0)}{2\pi\,\mathrm{d}x}$$

Rearranging in terms of q provides:

$$q = -\frac{2\pi G u_x\,\mathrm{d}x}{\ln(r_1/r_0)} \tag{A-4}$$

Substituting Eq. (A-3) and Eq. (A-4) into Eq. (A-1) provides:

$$\pi r_0^2\,\mathrm{d}\sigma - \frac{2\pi G u_x\,\mathrm{d}x}{\ln(r_1/r_0)} = 0 \tag{A-5}$$

$$\mathrm{d}\sigma = \frac{2G u_x\,\mathrm{d}x}{r_0^2\ln(r_1/r_0)}$$

The total fiber deformation at x equals the matrix shear deformation u_x. Therefore the tensile strain in increment $\mathrm{d}x$ is:

$$\mathrm{d}u_x/\mathrm{d}x = \sigma/E \tag{A-6}$$

Differentiating Eq. (A-5) gives:

$$\frac{\mathrm{d}^2\sigma}{\mathrm{d}x^2} = \frac{2G(\mathrm{d}u_x/\mathrm{d}x)}{r_0^2\ln(r_1/r_0)}$$

Substituting the above expression into Eq. (A-6) provides:

$$\frac{\mathrm{d}^2\sigma}{\mathrm{d}x^2} = \frac{(2G/E)\sigma}{r_0^2\ln(r_1/r_0)}$$

or:

$$\frac{\mathrm{d}^2\sigma}{\mathrm{d}x^2} - \frac{(2G/E)\sigma}{r_0^2\ln(r_1/r_0)} = 0 \tag{A-7}$$

If we let:

$$\alpha^2 = (2G/E)/r_0^2\ln(r_1/r_0) \tag{A-8}$$

then by operator notation Eq. (A-7) becomes:

$$(D^2 - \alpha^2)\sigma = 0 \tag{A-9}$$

solving Eq. (A-9) by standard methods we obtain:

$$\sigma = C_1 \exp(-\alpha x) + C_2 \exp(\alpha x) \tag{A-10}$$

Since $\sigma = 0$ at high negative values of x we obtain:

$$C_1 = 0$$

$$C_2 = P/\pi r_0^2$$

Differentiating Eq. (A-10) we obtain:

$$\frac{d\sigma}{dx} = C_2 \alpha \exp(\alpha x) = \frac{\alpha P \exp(\alpha x)}{\pi r_0^2} \tag{A-11}$$

Recall that the shear stress at the fiber surface λ_{r_0} is:

$$\lambda_{r_0} = \frac{(-q/dx)}{2\pi r_0}$$

and

$$-q/dx = 2\pi Gu / \ln(r_1/r_0)$$

Combining these relations provides:

$$\lambda_{r_0} = Gu_x / r_0 \ln(r_1/r_0) \tag{A-12}$$

Substituting Eq. (A-12) into Eq. (A-5) provides:

$$\frac{d\sigma}{dx} = \frac{2Gu_x}{r_0^2 \ln(r_1/r_0)} = \frac{2\lambda_{r_0}}{r_0} \tag{A-13}$$

Combining Eq. (A-11) and Eq. (A-13) provides:

$$\lambda_{r_0} = \frac{\alpha P \exp(\alpha x)}{2\pi r_0} \tag{A-14}$$

For the boundary condition $x = 0$, $r = r_0$, Eq. (A-14) becomes:

$$\lambda_0 = \alpha P / 2\pi r_0 \tag{A-15}$$

Equation (A-14) is considered, within the frame of the simplifying assumptions, a general expression for fiber-matrix shear stress for all values of $x \leqslant 0$.

References

1. A. H. Cottrell, *Proc. Roy. Soc.* **A282**, 2 (1964).
2. G. A. Cooper, and A. Kelly, *J. Mechanics and Phys. of Solids* **15**, 279 (1967).
3. G. A. Cooper, and A. Kelly, in *Interfaces in Composites*, ASTM STP 452 (1969), pp. 90–106.

4. A. Kelly, *Proc. Roy. Soc.* **A319**, 95 (1970).
5. J. O. Outwater, and J. C. Murphy, 26th Annual Tech, Conf.. Reinf. Plastics/Composites Div., Soc. of Plastics Industry (1969), Paper 11-C.
6. L. B. Greszczuk, in *Interfaces in Composites*, ASTM STP 452 (1969), pp. 42–58.
7. P. Lawrence, *J. Materials Sci.* **7**, 1 (1972).
8. T. H. Lin, D. Salinas and Y. M. Ito, *Ibid.* **6**, 48 (1972).
9. B. Harris, P. W. R. Beaumont and E. M. de Ferran, *J. Materials Sci.* **6**, 238 (1971).
10. J. Fitz-Randolph, D. C. Phillips, P. W. R. Beaumont and A. S. Tetelman, *Ibid.* **7**, 1 (1972).
11. L. J. Broutmann, in *Interfaces in Composites*, ASTM STP 452 (1969), pp. 27–41.
12. M. J. Salkind, *Ibid*, pp. 1–2.